

Letter

Open Access

Xiaoyu Yang, Xiaoyong Hu*, Hong Yang and Qihuang Gong

Ultracompact all-optical logic gates based on nonlinear plasmonic nanocavities

DOI 10.1515/nanoph-2016-0118

Received May 16, 2016; revised August 11, 2016; accepted August 15, 2016

Abstract: In this study, nanoscale integrated all-optical XNOR, XOR, and NAND logic gates were realized based on all-optical tunable on-chip plasmon-induced transparency in plasmonic circuits. A large nonlinear enhancement was achieved with an organic composite cover layer based on the resonant excitation-enhancing nonlinearity effect, slow light effect, and field confinement effect provided by the plasmonic nanocavity mode, which ensured a low excitation power of 200 μW that is three orders of magnitude lower than the values in previous reports. A feature size below 600 nm was achieved, which is a one order of magnitude lower compared to previous reports. The contrast ratio between the output logic states “1” and “0” reached 29 dB, which is among the highest values reported to date. Our results not only provide an on-chip platform for the study of nonlinear and quantum optics but also open up the possibility for the realization of nanophotonic processing chips based on nonlinear plasmonics.

Keywords: all-optical logic gates; plasmon-induced transparency; third-order optical nonlinearity.

PACS numbers: 42.65.Hw; 78.67-n; 81.07.Pr.

1 Introduction

Recently, nanoscale all-optical logic gate devices have attracted enormous attention because of their important applications in the fields of optical computing systems and optical interconnection networks. All-optical logic gates can be divided into basic logic gates (AND, OR, and NOT gates) and complex logic gates (XNOR, NOR, NAND, and XOR gates) [1, 2]. The fundamental concept for realizing basic all-optical logic gates is to use the magneto-optic effect in bulk ferromagnetic crystals [3, 4], the electro-optic effect in bulk periodically poled lithium niobate crystals [5], and the linear interference of light propagating in photonic microstructures [6–9]. However, the large size of the bulk ferromagnetic and lithium niobate crystals, of the order of several millimeters, is unsuitable for practical chip-integrated applications [10, 11]. Various schemes have been proposed to demonstrate all-optical basic logic gates based on linear interference mechanisms (or third-order nonlinear optical effects) in photonic microstructures and plasmonic nanostructures, such as photonic crystals [12–23], microring resonators [24–30], nano-bridges [31], graphene-oxide films [32, 33], photonic and plasmonic nanowires [34–36], metamaterials [37–39], and semiconductor optical amplifiers [40, 41]. The extremely high requirements placed on the light paths for the linear interference mechanism and relatively small third-order nonlinear susceptibility of conventional materials result in a low output logic state contrast of <10 dB and high signal intensities of several GW/cm^2 for basic all-optical logic gates. Fu et al. have pointed out that it is possible to realize cascaded complex all-optical logic devices based on third-order nonlinear optical effects [42]. However, to date, there has been little experimental progress in achieving complex logic gates based on nonlinear optical effects; the limitations of current nonlinear materials are the bottleneck in this process [43, 44]. Zhou et al. realized OR and NOR logic gates based on a four-wave mixing process with an incident signal light intensity of $1 \text{ GW}/\text{cm}^2$ [45]. Additionally, Fu et al. reported all-optical XNOR and XOR gates in nanoscale plasmonic slot waveguides with a high-intensity contrast ratio of 24 dB between the output

*Corresponding author: Xiaoyong Hu, State Key Laboratory for Mesoscopic Physics and Department of Physics, Collaborative Innovation Center of Quantum Matter, Peking University, Beijing 100871, P.R. China; and Collaborative Innovation Center of Extreme Optics, Shanxi University, Taiyuan 030006, P.R. China, e-mail: xiaoyonghu@pku.edu.cn

Xiaoyu Yang: State Key Laboratory for Mesoscopic Physics and Department of Physics, Collaborative Innovation Center of Quantum Matter, Peking University, Beijing 100871, P.R. China

Hong Yang and Qihuang Gong: State Key Laboratory for Mesoscopic Physics and Department of Physics, Collaborative Innovation Center of Quantum Matter, Peking University, Beijing 100871, P.R. China; and Collaborative Innovation Center of Extreme Optics, Shanxi University, Taiyuan 030006, P.R. China

logic states “1” and “0”; however, this process requires complicated and extremely precise microfabrications [42]. It is therefore still a significant challenge to realize ultracompact complex logic gates with high contrast ratios between the output logic states “1” and “0” based on third-order nonlinear optical effects.

Here, we realized nanoscale integrated all-optical XNOR, XOR, and NAND logic gates in plasmonic nanostructures based on the incident light-induced shift of plasmonic nanocavity modes and the plasmon-induced transparency (PIT) window by directly using the third-order nonlinear optical Kerr effect in plasmonic circuits. The plasmonic nanostructure consisted of a plasmonic waveguide side-coupled to a single plasmonic nanocavity (or two plasmonic asymmetric nanocavities) covered with a nonlinear organic composite layer made of poly[2-methoxy-5-(2-ethylhexyloxy)-1,4-phenylenevinylene] doped with laser dye IR140 (MEH-PPV:IR140). The PIT window was formed via interference coupling between two excitation pathways (i.e. by exciting the nanocavity C1 and C2 modes) by the surface plasmon polariton (SPP) propagating in the plasmonic waveguide [46, 47]. A large nonlinear enhancement is achieved with the organic composite MEH-PPV:IR140 cover layer based on the resonant excitation-enhancing nonlinearity effect, slow light effect, and field confinement effect provided by the plasmonic nanocavity mode, which ensures a low excitation power of 200 μ W. A feature size below 600 nm was achieved, which is one order of magnitude lower compared to previously reported values. The contrast ratio between the output logic states “1” and “0” reached 20 dB, which is among the highest values reported so far. Thus, our results can be used to not only provide an on-chip platform for the study of nonlinear and quantum optics but also open up the possibility for the realization of nanophotonic processing chips based on nonlinear plasmonics.

2 Results and discussion

The schematic structure of the plasmonic nanostructure, which consists of a plasmonic waveguide side-coupled to plasmonic nanocavity C1, is shown in Figure 1A without the MEH-PPV:IR140 cover layer. The plasmonic waveguide was constructed from an air nanogroove with a width of 150 nm and a depth of 150 nm etched in a 300-nm-thick gold film deposited on a silicon dioxide substrate. The plasmonic nanocavity C1 was formed by a nanogroove with length, width, and depth of 350, 150, and 150 nm etched in the 300-nm-thick gold film. The 300-nm-thick

gold films were fabricated using a laser molecular beam epitaxy growth system (Model LMBE 450; SKY Company, China). The beam (with a wavelength of 248 nm, pulse width of 25 ns, and pulse repetition rate of 5 Hz) output from an excimer laser system (Model COMPEXPro 205; Coherent Company, USA) was focused on a gold target mounted on a rotating holder, situated 17 mm away from the silicon dioxide substrates. The typical energy density of the excitation laser was 430 mJ/cm². Then, a focused ion beam etching system (Model Helios NanoLab 600; FEI Company, USA) was used to prepare the logic gate patterns. To excite and collect the needed SPP mode, we also etched a coupling grating connected with an air groove with a triangular configuration at the input port of each plasmonic slot waveguide. We also etched a grating in the output port to help couple the SPP mode to free space for the purpose of the measurement. A scanning electron microscopy (SEM) image of the plasmonic nanostructure, which consisted of a plasmonic waveguide side-coupled to plasmonic nanocavity C1, is shown in Figure 1B without the MEH-PPV:IR140 cover layer. Finally, spin coating was used to fabricate the 100-nm-thick MEH-PPV:IR140 cover layer on the surface of the plasmonic nanostructure. We measured the linear spectrum of the plasmonic waveguide, which was side-coupled to plasmonic nanocavity C1 and had an MEH-PPV:IR140 cover layer, using a nanospectroscopy measurement system [47]; the measured results are shown in Figure 1C. In our experiment, a p-polarized CW Ti:sapphire laser system (Model Mira 900F; Coherent Company, USA) was used as the light source. The line width of the laser spectrum of an 800 nm incident CW laser was only 1.6 nm, which guaranteed that only the desired quasi-monochromatic SPP mode could be excited in the plasmonic waveguide. The coupling grating was normally illuminated from the back side. The optically thick gold film prohibited direct transmission of the incident light. The SPP mode propagating through the plasmonic waveguide was scattered by the decoupling grating. The scattered light was collected using a long working distance objective (Mitutoyo 20; NA = 0.58) and then detected by a charge-coupled device (CCD). The measured transmission was normalized with respect to a reference waveguide that had the same structural parameters but was not coupled to the plasmonic nanocavity C1. This is the normal method widely used to study the transmission properties of plasmonic nanostructures [47].

It is very clear from Figure 1C that a transmission dip appeared in the linear transmission spectrum. The wavelength of the minimum transmission (900 nm) corresponds to the resonant wavelength of the plasmonic nanocavity C1 [47]. The measured results are in agreement with

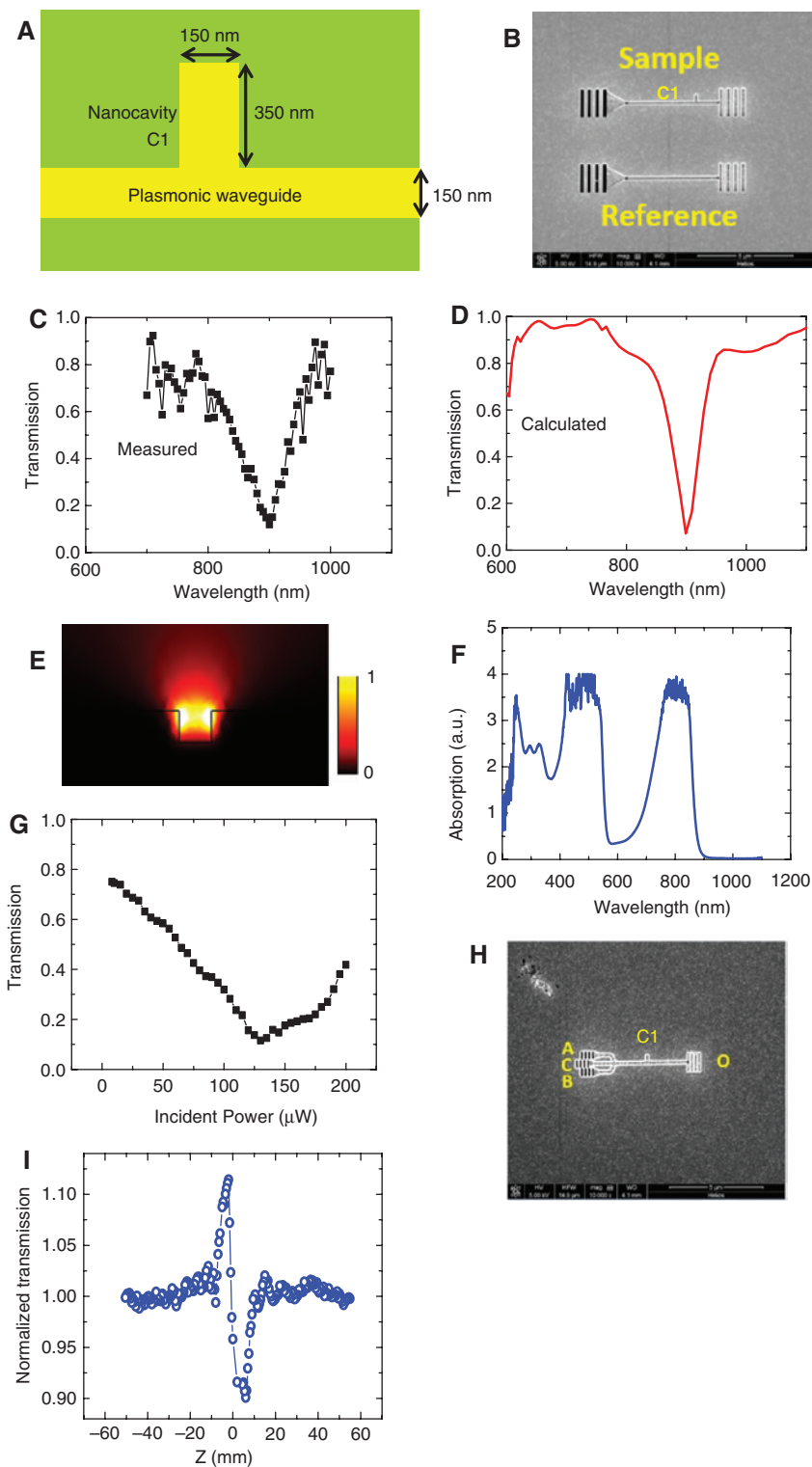


Figure 1: Characterization of the plasmonic nanocavity sample and the optical nonlinearity of MEH-PPV:IR140.

(A) Schematic structure of the plasmonic waveguide side-coupled to plasmonic nanocavity C1 without the MEH-PPV:IR140 cover layer. (B) SEM image of the plasmonic waveguide side-coupled to a plasmonic nanocavity and the reference waveguide without the MEH-PPV:IR140 cover layer. Measured (C) and calculated (D) linear spectra of plasmonic waveguide side-coupled to plasmonic nanocavity C1 with the MEH-PPV:IR140 cover layer. (E) Calculated power density profile of the SPP mode in nanocavity C1 excited by an 800 nm incident light. (F) Measured linear absorption spectrum of 100-nm-thick MEH-PPV:IR140 film. (G) Measured transmission changes of an 830 nm 120 fs incident light propagating through the plasmonic waveguide side-coupled to plasmonic nanocavity C1 with the MEH-PPV:IR140 cover layer as a function of the incident power. (H) SEM image of the plasmonic sample without coating the MEH-PPV:IR140 cover layer for the performance of all-optical XNOR logic gate function. (I) Measured closed-aperture Z-scan curve of a 100-nm-thick MEH-PPV:IR140 film under excitation of an 830 nm 120 fs 86 MHz laser beam.

the ones calculated via the finite element method (using the commercial software package COMSOL Multiphysics) [47], as shown in Figure 1D. The complex dielectric function of gold was taken from results reported by Johnson and Christy [48]. We also calculated the power density profile of the SPP mode in the nanocavity C1 excited by incident light with a wavelength of 800 nm, and the calculated result is shown in Figure 1E. The guided SPP mode was mainly confined in the nanogroove region, although it also extended into the upper MEH-PPV:IR140 cover layer, which is in agreement with the calculations of Li et al. [49]. This indicates that the resonance properties of the plasmonic nanocavity C1 were very sensitive to the refractive index change of the MEH-PPV:IR140 cover layer. We also measured the linear absorption spectrum of a 100-nm-thick MEH-PPV:IR140 composite film using a visible-near-infrared absorption spectrum measurement system (LABRAM-HR800, Horiba, Japan), and the measured results are shown in Figure 1F. They show a broad linear absorption band ranging from 700 to 900 nm, which originates from the linear absorption of IR140. Therefore, for an incident signal light whose wavelength is located near 800 nm, the third-order nonlinearity of the MEH-PPV:IR140 cover layer can be greatly enhanced using the resonant excitation-enhancing nonlinearity effect and the field reinforcement effect provided by the plasmonic nanocavity mode. To confirm the all-optical tunability of the plasmonic nanocavity C1, we measured the transmission changes of a 120-fs-long 830 nm incident light pulse propagating through the plasmonic waveguide side-coupled to plasmonic nanocavity C1 (with the MEH-PPV:IR140 cover layer) as a function of the incident power using the nanospectroscopy measurement system. With increasing incident power, the transmission of the 830 nm signal light decreased. The wavelength of 830 nm was located at the edge of the pass band in the linear transmission spectrum of the plasmonic waveguide side-coupled to nanocavity C1, as shown in Figure 1C and D. Jiang et al. have pointed out that the organic composite MEH-PPV:IR140 has a negative nonlinear refractive index under resonant excitation [50], which causes the refractive index of the organic composite MEH-PPV:IR140 to decrease with increasing incident power levels. As a result, the resonant wavelength of the nanocavity C1 mode shifts toward shorter wavelengths, and the transmission at 830 nm decreases. When the incident power was increased to 125 μ W, the transmission at 830 nm decreased to 10%. Additionally, when the incident power was increased to 125 μ W, the resonant wavelength of the nanocavity C1 shifted to 830 nm. When the incident power was above 130 μ W, the transmission at 830 nm increased,

and the resonant wavelength of the nanocavity C1 shifted to wavelengths lower than 830 nm. This indicates that the plasmonic nanocavity C1 has excellent all-optical tunability. The nonlinear enhancement factor for the SPP cavity could be estimated from the power density profile of the SPP mode in nanocavity C1 excited by incident light of 800 nm wavelength, as shown in Figure 1E. It is very clear that the power density distribution in the upper surface of the gold film around the SPP cavity was enhanced 70-fold compared to that of the region away from the SPP cavity. Therefore, a 70-fold nonlinear enhancement was obtained with the organic composite MEH-PPV:IR140 layer because of the field confinement effect provided by the plasmonic nanocavity mode. The quality factor Q of the SPP nanocavity mainly depended on the losses of the SPP nanocavity, including the intrinsic large ohmic losses of gold, the surface roughness of the fabricated SPP nanocavity, and the imperfectly etched nanocavity structure, which results in a relatively small quality factor Q of 10 for the SPP nanocavity, as shown in Figure 1C. This has been confirmed by measurements by Han et al. [51] and Chen et al. [52]. The Purcell factor F_p can be calculated using the following relation [53]:

$$F_p = \frac{3}{4\pi^2} \frac{Q}{V} \left(\frac{\lambda}{n} \right)^3 \quad (1)$$

where Q is the quality factor of the optical cavity, V is the mode volume of the optical cavity, λ is the spontaneous emission wavelength, and n is the refractive index of the material the optical cavity is made of. For the SPP nanocavity used in our experiment, the Purcell factor F_p was calculated to be 760. To check the feasibility of the nonlinear effect, we measured the closed-aperture Z-scan curve of a 100-nm-thick MEH-PPV:IR140 film under excitation of a 120-fs-long 830 nm 86 MHz laser beam, and the measured results are shown in Figure 1I. The measured nonlinear refractive index was -2.9×10^{-6} cm²/kW, which is five orders of magnitude higher compared to that of MEH-PPV under excitation of a 120-fs-long 830 nm 86 MHz laser beam (-7.2×10^{-11} cm²/kW) [54]. This confirms the feasibility of using the nonlinear effect of organic composite MEH-PPV:IR140. The physical mechanism of the all-optical logic function was realized based on the intensity-dependent resonance shift of a nonlinear material-loaded plasmonic nanocavity.

The plasmonic nanostructure sample for evaluating the performance of the all-optical XNOR logic gate function had three incident waveguides A, B, and C, one plasmonic nanocavity C1 side-coupled to a bus plasmonic waveguide, and an output plasmonic waveguide O, as shown

in Figure 1H. Waveguide C was used as the reference waveguide, which maintained the signal light input during the performance of the logic gate operation. To perform the logic operation “0 XNOR 0 = 1”, we etched only the input-coupling grating into reference waveguide C, as shown in Figure 2A. The measured CCD image under excitation of a 120-fs-long 830 nm 200 μ W laser is shown in Figure 2B. A strongly scattered signal with an intensity of 90 arbitrary units (au) was obtained from the CCD image, which corresponds to the output logic signal “1”. This is confirmed by the results calculated using the finite element method, as shown in Figure 2C. To perform the logic operation “1 XNOR 0 = 0”, we etched only the input-coupling grating into reference waveguide C and incident waveguide A, as shown in Figure 2D. The measured CCD image under excitation of a 120-fs-long 830 nm 200 μ W laser is shown in Figure 2E. The signal showed no signs of scattering and had an intensity of 0.12 au (obtained from the CCD image); this signal strength corresponds to the output logic signal “0”. This is confirmed by the results calculated using the finite element method, as shown in Figure 2F. To perform the logic operation of “0 XNOR 1 = 0”, we etched only the input-coupling grating into the reference waveguide C and incident waveguide B, as shown in Figure 2G. The measured CCD image under excitation of a 120-fs-long 830 nm 200 μ W laser is shown in Figure 2H. The signal showed no signs of scattering and had an intensity of 0.12 au (obtained from the CCD image); this intensity corresponds to the output logic signal “0”. This is confirmed by the results calculated using the finite element method, as shown in Figure 2I. To perform the logic operation of “1 XNOR 1 = 1”, we etched the input-coupling grating into reference waveguide C and incident waveguides A and B, as shown in Figure 2J. The measured CCD image under excitation of a 120-fs-long 830 nm 200 μ W laser is shown in Figure 2K. The signal showed no signs of scattering and had an intensity of 113 (obtained from the CCD image), which corresponds to the output logic signal “1”. This is confirmed by the results calculated using the finite element method, as shown in Figure 2L. Therefore, the output logic state contrast between “1” and “0” reached 29.7 dB, which is among the highest value reported to date [42–45]. The incident light intensity was 7.8 MW/cm², which is three orders of magnitude lower compared to previous reports [42–45]. To understand the physical mechanism, we calculated the linear transmission spectrum of the plasmonic waveguide side-coupled to plasmonic nanocavity C1 with the MEH-PPV:IR140 cover layer under different excitation conditions; the calculated results are shown in Figure 2M. According to our calculations, under excitation of signal light that propagated through reference waveguide C, the

position of C in the linear transmission spectrum shifted to 830 nm, which meant that a high transmission could be obtained at 830 nm. While under excitation of the signal light propagating through reference waveguide C and incident waveguide A (or B), the transmission minimum in the linear transmission spectrum shifted to 830 nm, which meant that a very low transmission could be obtained at 830 nm. Although under excitation of the signal light propagating through reference waveguide C and incident waveguides A and B, the position of C + A + B in the linear transmission spectrum shifted to 830 nm, which meant that a high transmission could once again be obtained at 830 nm.

The schematic structure of the plasmonic nanostructure consisting of the plasmonic waveguide side-coupled to plasmonic nanocavities C1 and C2 without the MEH-PPV:IR140 cover layer is shown in Figure 3A. The plasmonic nanocavity C2 was formed by a nanogroove with length, width, and depth of 300, 170, and 150 nm etched into the 300-nm-thick gold film. There was a distance of 290 nm between nanocavities C1 and C2. Figure 3C shows the measured linear transmission spectrum of the plasmonic waveguide side-coupled to plasmonic nanocavities C1 and C2 (with the MEH-PPV:IR140 cover layer), as shown in Figure 3B. A transmission peak appeared in the transmission forbidden band, which indicates the formation of PIT. The central wavelength and transmission of the transparency window were 850 nm and 82%, which is in agreement with the results calculated using the finite element method, as shown in Figure 3D. The PIT window originates from the interference coupling between two excitation pathways (excitation of the nanocavity C1 and C2 modes) by the SPP propagating in the plasmonic waveguide [46, 47]. The plasmonic nanostructure consisting of the plasmonic waveguide side-coupled to plasmonic nanocavities C1 and C2 with the MEH-PPV:IR140 cover layer could be used to demonstrate the operation of the XOR logic gate. The plasmonic nanostructure sample had two input plasmonic waveguides A and B, one bus plasmonic waveguide side-coupled to nanocavities C1 and C2, and one output plasmonic waveguide O, as shown in Figure 3E. The incident signal wavelength was set to 850 nm. To perform the logic operation “1 XOR 0 = 1”, we etched only the input-coupling grating into input waveguide A, as shown in Figure 3F. The measured CCD image under excitation of a 120-fs-long 850 nm 180 μ W laser is shown in Figure 2G. A strongly scattered signal with an intensity of 80 au was obtained from the CCD image, which corresponds to the output logic signal “1”. This is confirmed by the results calculated using the finite element method, as shown in Figure 3H. To perform the logic operation of “0 XOR

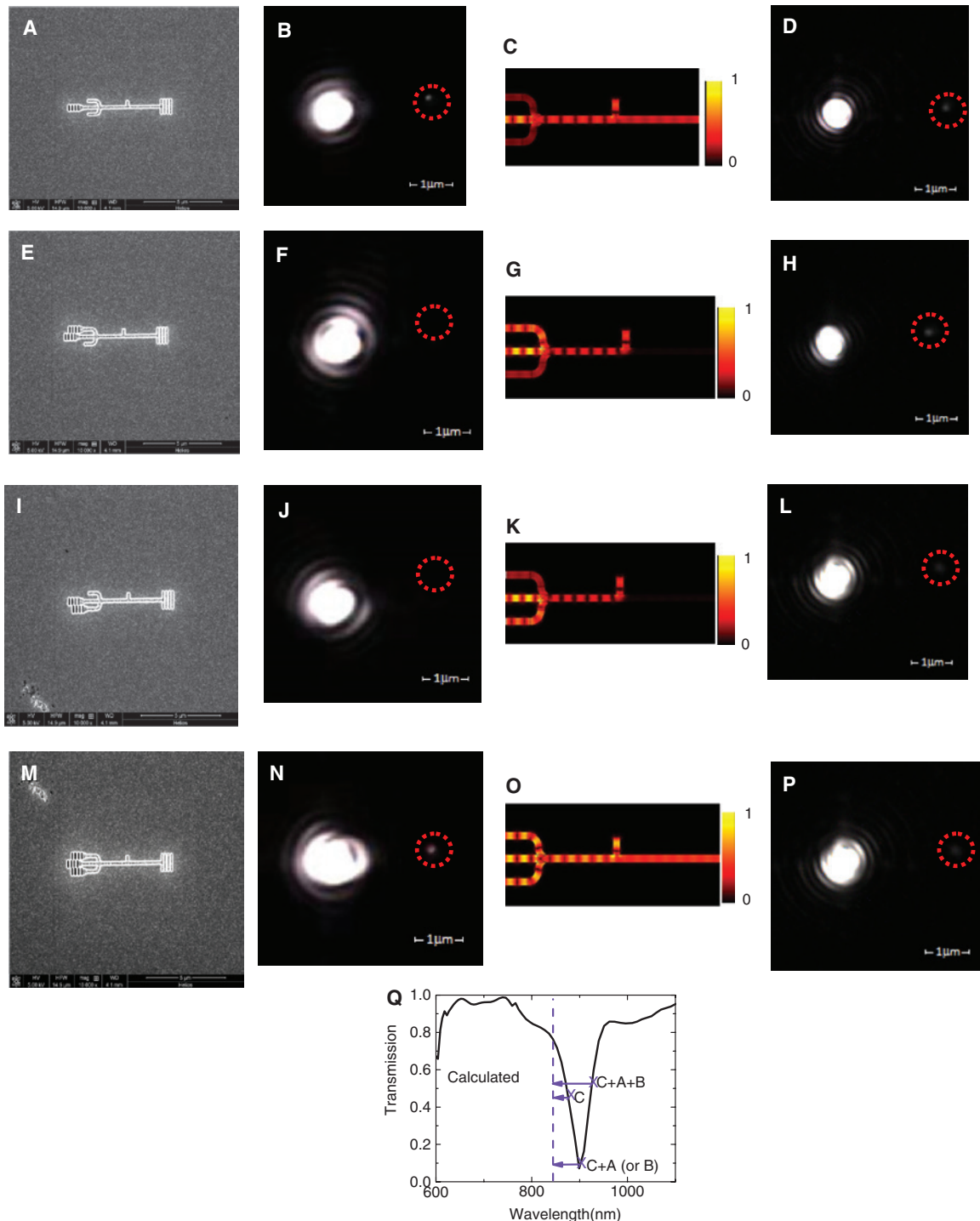


Figure 2: Logic operation of XNOR gate.

SEM image of plasmonic sample without coating the MEH-PPV:IR140 cover layer (A), measured CCD image under excitation of an 830 nm 120 fs laser (B), calculated results (C), and measured CCD image of the control sample (D) for the logic operation of “0 XNOR 0=1”. SEM image of plasmonic sample without coating the MEH-PPV:IR140 cover layer (E), measured CCD image under excitation of an 830 nm 120 fs laser (F), calculated results (G), and measured CCD image of the control sample (H) for the logic operation of “1 XNOR 0=0”. SEM image of plasmonic sample without coating the MEH-PPV:IR140 cover layer (I), measured CCD image under excitation of an 830 nm 120 fs laser (J), calculated results (K), and measured CCD image of the control sample (L) for the logic operation of “0 XNOR 1=0”. SEM image of plasmonic sample without coating the MEH-PPV:IR140 cover layer (M), measured CCD image under excitation of an 830 nm 120 fs laser (N), calculated results (O), and measured CCD image of the control sample (P) for the logic operation of “1 XNOR 1=1”. The red dashed circle indicates the position of the decoupling grating. (Q) Calculated linear transmission spectrum of a plasmonic waveguide side-coupled to plasmonic nanocavity C1 with the MEH-PPV:IR140 cover layer under different excitation cases. Crosses indicate which points shift to the position of 830 nm.

1=1", we etched only the input-coupling grating into input waveguide B, as shown in Figure 3I. The measured CCD image under excitation of a 120-fs-long 850 nm 180 μ W laser is shown in Figure 2J. A strongly scattered signal with an intensity of 83 au was obtained from the CCD image, which corresponds to the output logic signal "1". This is confirmed by the results calculated using the finite element method, as shown in Figure 3K. To perform the logic operation of "1 XOR 1=0", we etched the input-coupling grating into input waveguides A and B, as shown in Figure 3L. The measured CCD image under excitation of a 120-fs-long 850 nm 180 μ W laser is shown in Figure 2M. A very weakly scattered signal with an intensity of 0.14 au was obtained from the CCD image, which corresponds to the output logic signal "0". This is confirmed by the results calculated using the finite element method, as shown in Figure 3N. Therefore, the output logic state contrast between "1" and "0" reached 27.7 dB. To understand the physical mechanism, we calculated the linear transmission spectrum of the plasmonic waveguide side-coupled to nanocavities C1 and C2 with the MEH-PPV:IR140 cover layer under different excitation conditions; the calculated results are shown in Figure 3O. According to our calculations, under excitation of the signal light propagating through the incident waveguide A (or B), the wavelength of 850 nm still fell within the transparency window region, which ensured that there was a high transmission at 850 nm. Although under excitation of the signal light propagating through the incident waveguides A and B, the position of the transmission minimum in the linear transmission spectrum shifted to the position of 850 nm, which causes a low transmission at 850 nm.

The plasmonic nanostructure consisting of the plasmonic waveguide side-coupled to plasmonic nanocavities C1 and C2 with the MEH-PPV:IR140 cover layer could also be used to demonstrate the operation of the NAND logic gate. The plasmonic nanostructure sample had two input plasmonic waveguides A and B, one reference waveguide C, one bus plasmonic waveguide side-coupled to nanocavities C1 and C2, and one output plasmonic waveguide O, as shown in Figure 4A. The incident signal wavelength was set to 815 nm. To perform the logic operation of "0 NAND 0=1", we etched only the input-coupling grating into reference waveguide C, as shown in Figure 4B. The measured CCD image under excitation of a 120-fs-long 815 nm 180 μ W laser is shown in Figure 4C. A strongly scattered signal with an intensity of 85 au was obtained from the CCD image, which corresponds to the output logic signal "1". This is confirmed by the results calculated using the finite element method, as shown in Figure 4D. To perform the logic operation of "1 NAND 0=1", we

etched only the input-coupling grating in reference waveguide C and incident waveguide A, as shown in Figure 4E. The measured CCD image under excitation of a 120-fs-long 815 nm 180 μ W laser is shown in Figure 4F. A strongly scattered signal with an intensity of 83 au was obtained from the CCD image, which corresponds to the output logic signal "1". This is confirmed by the results calculated using the finite element method, as shown in Figure 4G. To perform the logic operation of "0 NAND 1=1", we etched only the input-coupling grating into reference waveguide C and incident waveguide B, as shown in Figure 4H. The measured CCD image under excitation of a 120-fs-long 815 nm 180 μ W laser is shown in Figure 4I. A strongly scattered signal with an intensity of 84 au was obtained from the CCD image, which corresponds to the output logic signal "1". This is confirmed by the results calculated using the finite element method, as shown in Figure 4J. To perform the logic operation of "1 NAND 1=0", we etched the input-coupling grating into reference waveguide C and incident waveguides A and B, as shown in Figure 4K. The measured CCD image under excitation of a 120-fs-long 815 nm 180 μ W laser is shown in Figure 4L. Very weakly scattered signal with an intensity of 0.15 au was obtained from the CCD image, which corresponds to the output logic signal "0". This is confirmed by the results calculated using the finite element method, as shown in Figure 4M. Therefore, the output logic state contrast between "1" and "0" reached 27.5 dB. To understand the physical mechanism, we calculated the linear transmission spectrum of a plasmonic waveguide side-coupled to a plasmonic nanocavity with an MEH-PPV:IR140 cover layer under different excitation conditions, and the calculated results are shown in Figure 4N. According to our calculations, under excitation of the signal light propagating through reference waveguide C, the transparency window center shifted to 815 nm, which means that a high transmission can be obtained at 815 nm. Although under excitation of the signal light propagating through reference waveguide C and incident waveguide A (or B), the wavelength of 815 nm still fell within the transparency window region, which ensured a high transmission at 815 nm. Although under excitation of the signal light propagating through reference waveguide C and incident waveguides A and B, the transmission minimum in the linear transmission spectrum was shifted to 815 nm, which caused a low transmission at 815 nm. Hahn et al. have pointed out that, for an organic composite made of IR140 dye-doped polymer film, the bleaching of IR140 could be neglected for a weak excitation light source with an intensity far below 1 MW/cm², as the bleaching of IR140 occurs when the excitation light intensity is larger than 4 MW/cm² [55].

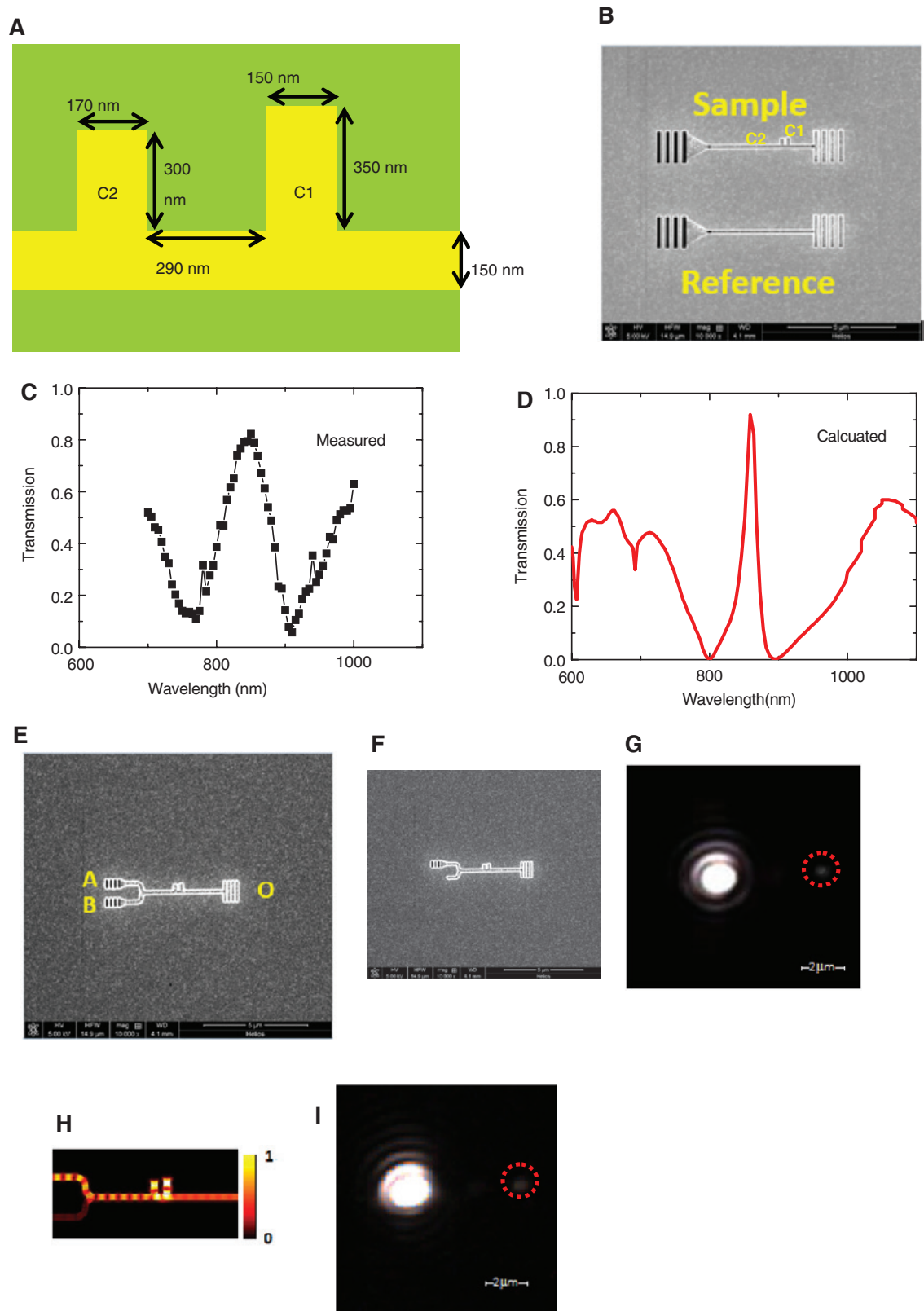


Figure 3: (Continued)

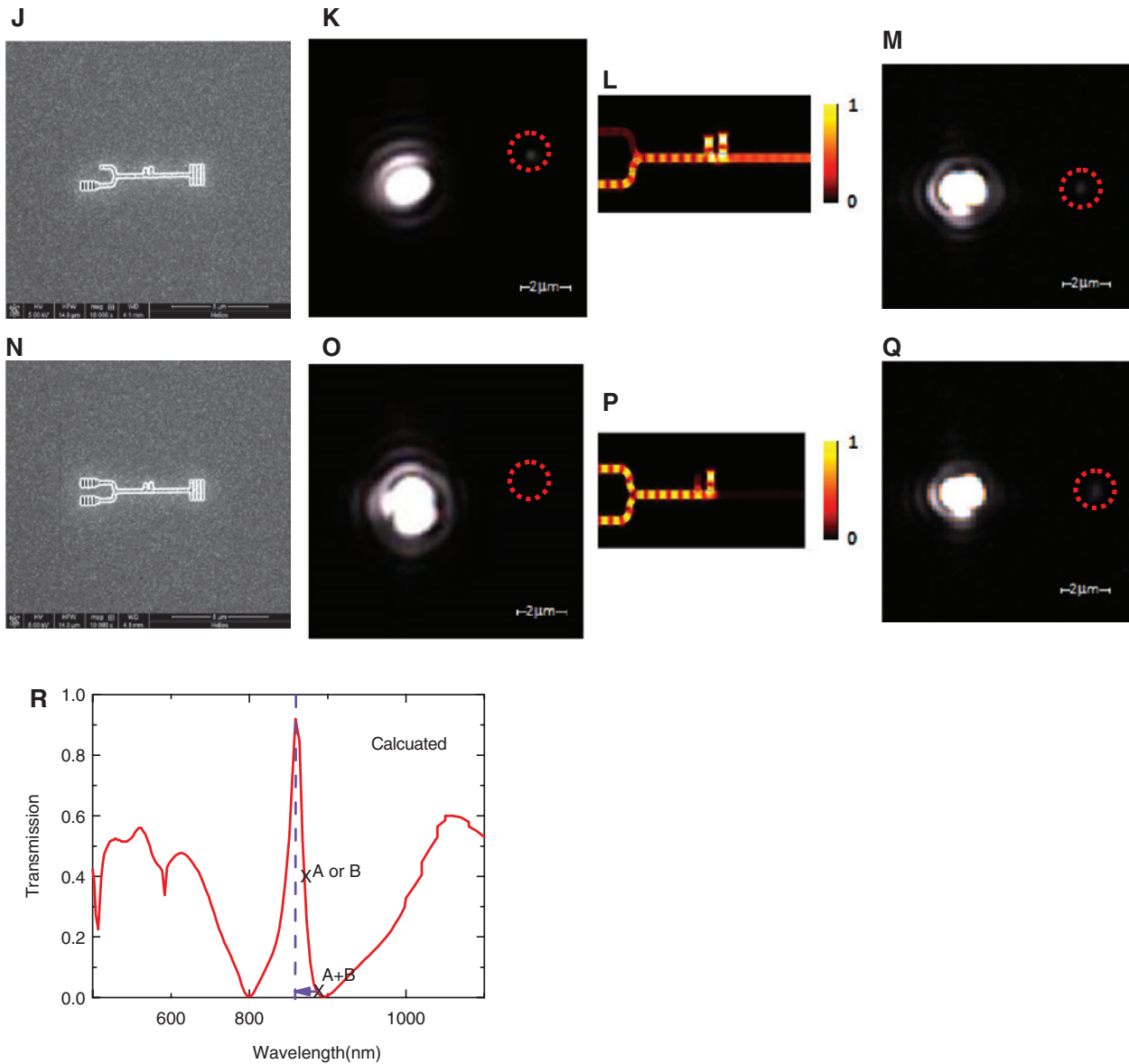


Figure 3: Logic operation of XOR gate.

(A) Schematic structure of the plasmonic waveguide side-coupled to plasmonic nanocavities C1 and C2 without the MEH-PPV:IR140 cover layer. (B) SEM image of the plasmonic waveguide side-coupled to plasmonic nanocavities C1 and C2 and the reference waveguide without the MEH-PPV:IR140 cover layer. Measured (C) and calculated (D) linear spectra of the plasmonic waveguide side-coupled to plasmonic nanocavities C1 and C2 with the MEH-PPV:IR140 cover layer. (E) SEM image of the plasmonic sample without coating the MEH-PPV:IR140 cover layer for the performance of all-optical XOR logic gate function. SEM image of plasmonic sample without coating the MEH-PPV:IR140 cover layer (F), measured CCD image under excitation of an 850 nm 120 fs laser (G), calculated results (H), and measured CCD image of the control sample (I) for the logic operation of “1 XOR 0 = 1”. SEM image of plasmonic sample without coating the MEH-PPV:IR140 cover layer (J), measured CCD image under excitation of an 850 nm 120 fs laser (K), calculated results (L), and measured CCD image of the control sample (M) for the logic operation of “0 XOR 1 = 1”. SEM image of plasmonic sample without coating the MEH-PPV:IR140 cover layer (N), measured CCD image under excitation of an 850 nm 120 fs laser (O), calculated results (P), and measured CCD image of the control sample (Q) for the logic operation of “1 XOR 1 = 0”. The red dashed circle indicates the position of the decoupling grating. (R) Calculated linear transmission spectrum of a plasmonic waveguide side-coupled to plasmonic nanocavity with the MEH-PPV:IR140 cover layer under different excitation cases. Crosses indicate which points shift to the position of 850 nm.

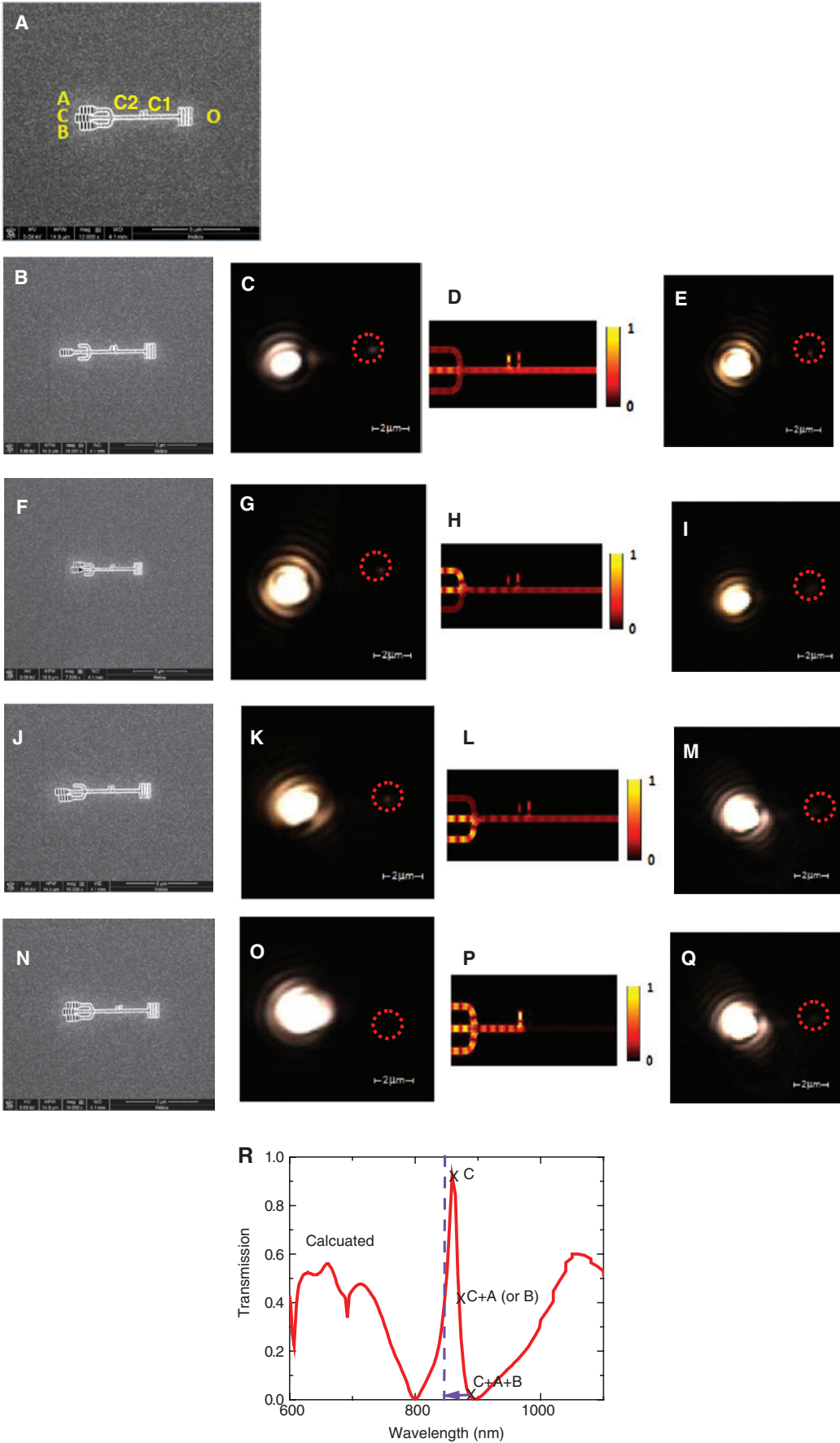


Figure 4: Logic operation of NAND gate.

(A) SEM image of the plasmonic sample without coating the MEH-PPV:IR140 cover layer for the performance of all-optical NAND logic gate function. SEM image of plasmonic sample without coating the MEH-PPV:IR140 cover layer (B), measured CCD image under excitation of an 815 nm 120 fs laser (C), calculated results (D), and measured CCD image of the control sample (E) for the logic operation of “0 NAND 0 = 1”. SEM image of plasmonic sample without coating the MEH-PPV:IR140 cover layer (F), measured CCD image under excitation of an 815 nm 120 fs laser (G), calculated results (H), and measured CCD image of the control sample (I) for the logic operation of “1 NAND 0 = 1”. SEM image of plasmonic sample without coating the MEH-PPV:IR140 cover layer (J), measured CCD image under excitation of an 815 nm 120 fs laser (K), calculated results (L), and measured CCD image of the control sample (M) for the logic operation of “0 NAND 1 = 1”. SEM image of plasmonic sample without coating the MEH-PPV:IR140 cover layer (N), measured CCD image under excitation of an 815 nm 120 fs laser (O), calculated results (P), and measured CCD image of the control sample (Q) for the logic operation of “1 NAND 1 = 0”. The red dashed circle indicates the position of the decoupling grating. (R) Calculated linear transmission spectrum of a plasmonic waveguide side-coupled to a plasmonic nanocavity with the MEH-PPV:IR140 cover layer under different excitation cases. Crosses indicate which points shift to the position of 815 nm.

In our experiment, the maximum signal light intensity reaching the position of the plasmonic nanocavities was about 700 kW/cm² because of the low input-coupling efficiency (<10%) of the input-coupling gratings in the input port of the plasmonic waveguides. Moreover, the experimental measurements of the sample lasted for 1 month, and perfect logic operations were obtained. Therefore, the bleaching of the laser dye IR140 could be neglected. The input grating couplers control whether light was coupled into the respective waveguide arm. There existed the cross-coupling for a case where the input grating coupler was omitted in the input waveguides. This only weakened the signal light intensity reaching the plasmonic nanocavities, and perfect logic operations were achieved according to our calculations and experiment measurements, as shown in the calculated logic operations in Figures 2–4. Because all the input grating couplers had the same structural parameters, and all the input grating couplers were evenly excited, the coupling into the waveguide from each input grating coupler was excited similarly.

3 Conclusion

In conclusion, we have experimentally realized ultracompact chip-integrated all-optical XNOR, XOR, and NAND logic gates in plasmonic circuits. A low threshold power of 200 μW, a small feature size of <600 nm, and a high contrast ratio between the output logic states “1” and “0” of 29 dB were obtained simultaneously. This not only provides an on-chip platform for the study of nonlinear and quantum optics but also opens up the possibility for the realization of nanophotonic processing chips based on nonlinear plasmonics.

Acknowledgments: This work was supported by the 973 Program of China under grant nos. 2013CB328704 and 2014CB921003 and the National Natural Science

Foundation of China under grant nos. 11225417, 61475003, 11134001, 11121091, 11527901, and 90921008.

References

- [1] Rani P, Kalra Y, Sinha RK. Design and analysis of polarization independent all-optical logic gates in silicon-on-insulator photonic crystal. *Opt Commun* 2016;374:148–55.
- [2] Sharifi H, Hamidi SM, Navi K. A new design procedure for all-optical photonic crystal logic gates and functions based on threshold logic. *Opt Commun* 2016;370:231–8.
- [3] Zeng HT, Read D, O’Brien L, et al. Asymmetric magnetic NOT gate and shift registers for high density data storage. *Appl Phys Lett* 2010;96:262510.
- [4] Ding J, Kostylev M, Adeyeye O. Realization of a mesoscopic reprogrammable magnetic logic based on a nanoscale reconfigurable magnonic crystal. *Appl Phys Lett* 2012;100:073114.
- [5] Zhang YX, Chen YP, Chen XF. Polarization-based all-optical logic controlled-NOT, XOR, and XNOR gates employing electro-optic effect in periodically poled lithium niobate. *Appl Phys Lett* 2011;99:161117.
- [6] Asakawa K, Sugimoto Y, Watanabe Y, et al. Photonic crystal and quantum dot technologies for all-optical switch and logic device. *N J Phys* 2006;8:208.
- [7] Tang XF, Zhai YX, Sun L, et al. Implementation of a reconfigurable optical logic gate using a single I/Q modulator with direct detection. *IEEE Photon J* 2016;8:7802808.
- [8] Li ZJ, Chen ZW, Li BJ. Optical pulse controlled all-optical logic gates in SiGe/Si multimode interference. *Opt Express* 2005;13:1033–8.
- [9] Ginzburg P, Hayat A, Vishnyakov V, Orenstein M. Photonic logic by linear unidirectional interference. *Opt Express* 2009;17:4251–6.
- [10] Chattopadhyay T. Optical logic gates using binary decision diagram with mirrors. *Opt Laser Technol* 2013;54:159–69.
- [11] Ostatnický T, Shelykh IA, Kavokin AV. Theory of polarization-controlled polariton logic gates. *Phys Rev B* 2010;81:125319.
- [12] Li QL, Yuan HL. All-optical logic gates based on cross-phase modulation in an asymmetric coupler. *Opt Commun* 2014;319:90–4.
- [13] Baryshev AV, Khanikaev AB, Inoue M, et al. Resonant behavior and selective switching of stop bands in three-dimensional photonic crystals with inhomogeneous components. *Phys Rev Lett* 2007;99:063906.

- [14] Yanik MF, Fan SH, Soljacic M, Joannopoulos JD. All-optical transistor action with bistable switching in a photonic crystal cross-waveguide geometry. *Opt Lett* 2003;28:2506–8.
- [15] McCutcheon MW, Rieger GW, Young JF, Dalacu D, Poole PJ, Williams RL. All-optical conditional logic with a nonlinear photonic crystal nanocavity. *Appl Phys Lett* 2009;95:221102.
- [16] Ballarini D, De Giorgi M, Cancellieri E, et al. All-optical polariton transistor. *Nat Commun* 2013;4:1778.
- [17] Tripathy SK, Sahu S, Mohapatro C, Dash SP. Implementation of optical logic gates using closed packed 2D-photonic crystal structure. *Opt Commun* 2012;285:3234–7.
- [18] Zhu ZH, Ye WM, Ji JR, Yuan XD, Zen C. High-contrast light-by-light switching and AND gate based on nonlinear photonic crystals. *Opt Express* 2006;14:1783–8.
- [19] Zhang YL, Zhang Y, Li BJ. Optical switches and logic gates based on self-collimated beams in two-dimensional photonic crystals. *Opt Express* 2007;15:9287–92.
- [20] Notomi M, Tanabe T, Shinya A, et al. Nonlinear and adiabatic control of high-Q photonic crystal nanocavities. *Opt Express* 2007;15:17458–81.
- [21] Liu Q, Ouyang ZB, Wu CJ, Liu CP, Wang JC. All-optical half adder based on cross structures in two-dimensional photonic crystals. *Opt Express* 2008;16:18992–9000.
- [22] Belotti M, Galli M, Gerace D, et al. All-optical switching in silicon-on-insulator photonic wire nano-cavities. *Opt Express* 2010;18:1450–61.
- [23] Liu Y, Qin F, Meng ZM, Zhou F, Mao QH, Li ZY. All-optical logic gates based on two-dimensional low-refractive-index nonlinear photonic crystal slabs. *Opt Express* 2011;19:1945–53.
- [24] Rakshit JK, Roy JN. Micro-ring resonator based all-optical reconfigurable logic operations. *Opt Commun* 2014;321:38–46.
- [25] Fushimi A, Tanabe T. All-optical logic gate operating with single wavelength. *Opt Express* 2014;22:4466–79.
- [26] Miyoshi Y, Ikeda K, Tobioka H, Inoue T, Namiki S, Kitayama K. Ultrafast all-optical logic gate using a nonlinear optical loop mirror based multi-periodic transfer function. *Opt Express* 2008;16:2570–7.
- [27] Wu YD, Shih TT, Chen MH. New all-optical logic gates based on the local nonlinear Mach-Zehnder interferometer. *Opt Express* 2008;16:248–57.
- [28] Xu QF, Lipson M. All-optical logic based on silicon micro-ring resonators. *Opt Express* 2007;15:924–9.
- [29] Tao JF, Wu J, Cai H, et al. A nanomachined optical logic gate driven by gradient optical force. *Appl Phys Lett* 2012;100:113104.
- [30] Xu QF, Soref R. Reconfigurable optical directed-logic circuits using microresonator-based optical switches. *Opt Express* 2011;19:5244–59.
- [31] Oh JY, Islam MS. Nanobridge gate-all-around phototransistors for electro-optical OR gate circuit and frequency doubler applications. *Appl Phys Lett* 2014;104:022110.
- [32] Roy S, Yadav C. Femtosecond all-optical parallel logic gates based on tunable saturable to reverse saturable absorption in graphene-oxide thin films. *Appl Phys Lett* 2013;103:241113.
- [33] Kang JH, Sarkar D, Khatami Y, Banerjee K. Proposal for all-graphene monolithic logic circuits. *Appl Phys Lett* 2013;103:083113.
- [34] Wei H, Wang ZX, Tian XR, Kall M, Xu HX. Cascaded logic gates in nanophotonic plasmon networks. *Nat Commun* 2011;2:387.
- [35] Piccione B, Cho CH, van Vugt LK, Agarwal R. All-optical active switching in individual semiconductor nanowires. *Nat Nanotechnol* 2012;7:640–5.
- [36] Wei H, Li ZP, Tian XR, et al. Quantum dot-based local field imaging reveals plasmon-based interferometric logic in silver nanowire networks. *Nano Lett* 2011;11:471–5.
- [37] Zhu LQ, Wu GD, Zhou JM, Dou W, Zhang HL, Wan Q. Laser directly written junctionless in-plane-gate neuron thin film transistors with AND logic function. *Appl Phys Lett* 2013;102:043501.
- [38] Papaioannou M, Plum E, Valente J, Rogers ET, Zheludev NI. Two-dimensional control of light with light on metasurfaces. *Light Sci Appl* 2016;5:e16070.
- [39] Ota M, Sumimura A, Fukuhara M, Ishii Y, Fukuda M. Plasmonic multimode-interference-based logic circuit with simple phase adjustment. *Sci Rep* 2016;6:24546.
- [40] Kotb A, Alamer FA. Dispersion on all-optical logic XOR gate using semiconductor optical amplifier. *Opt Quant Electron* 2016;48:327.
- [41] Shehata MI, Mohammed NA. Design and optimization of novel two inputs optical logic gates (NOT, AND, OR and NOR) based on single commercial TW-SOA operating at 40 Gbit/s. *Opt Quant Electron* 2016;48:336.
- [42] Fu YL, Hu XY, Lu CC, Yue S, Yang H, Gong QH. Proposal for all-graphene monolithic logic circuits. *Nano Lett* 2012;12:5784–90.
- [43] Zhang Y, Chen Y, Chen X. Polarization-based all-optical logic controlled-NOT, XOR, and XNOR gates employing electro-optic effect in periodically poled lithium niobate. *Appl Phys Lett* 2011;99:161117.
- [44] Meiri M, Zalevsky Z. Nano electro-optical modulator and all-optical logic gate on a silicon chip. *J Nanophoton* 2011;5:051811.
- [45] Zhou ZF, Liu CJ, Fang YM, et al. Optical logic gates using coherent feedback. *Appl Phys Lett* 2012;101:191113.
- [46] Kekatpure RD, Barnard ES, Cai W, Brongersma ML. Phase-coupled plasmon-induced transparency. *Phys Rev Lett* 2010;104:243902.
- [47] Yang XY, Hu XY, Chai Z, Lu CC, Yang H, Gong QH. Tunable ultracompact chip-integrated multichannel filter based on plasmon-induced transparencies. *Appl Phys Lett* 2014;104:221114.
- [48] Johnson PB, Christy RW. Optical constants of the noble metals. *Phys Rev B* 1972;6:4370–9.
- [49] Li XE, Jiang T, Shen LF, Deng XH. Subwavelength guiding of channel plasmon polaritons by textured metallic grooves at telecom wavelengths. *Appl Phys Lett* 2013;102:031606.
- [50] Jiang P, Hu XY, Zhang JX, Yang H, Gong QH. Ultra-fast all-optical switching in MEH-PPV photonic crystals with resonantly enhanced nonlinearity. *Appl Phys B* 2010;99:187–90.
- [51] Han ZH, Garcia-Ortiz CE, Radko IP, Bozhevolnyi SI. Detuned-resonator induced transparency in dielectric-loaded plasmonic waveguides. *Opt Lett* 2013;38:875–7.
- [52] Chen JJ, Wang C, Zhang R, Xiao JH. Multiple plasmon-induced transparencies in coupled-resonator systems. *Opt Lett* 2012;37:5133–5.
- [53] Vesseur EJR, de Abajo FJG, Polman A. Broadband Purcell enhancement in plasmonic ring cavities. *Phys Rev B* 2010;82:165419.
- [54] Ma GH, Guo LJ, Mi J, et al. Investigations of third-order nonlinear optical response of poly (p-phenylenevinylene) derivatives by femtosecond optical Kerr effect. *Physica B* 2001;305:147–54.
- [55] Hahn C, Song SH, Oh CH, Berini P. Plasmonic gain in long-range surface plasmon polariton waveguides bounded symmetrically by dye-doped polymer. *Appl Phys Lett* 2015;107:121107.